First Extraction of Single Differential Cross-Sections on Argon for CC1μ2p0π Event Topologies in the MicroBooNE Detector

MICROBOONE-NOTE-1117-PUB

The MicroBooNE Collaboration*

May 27, 2022

Abstract

The precise measurement of cross-sections for a variety of interactions is critical to the success of forthcoming flagship neutrino experiments. Of special interest are neutrino interactions that leave the nucleus in a 2-particle 2-hole state (2p2h). This note will present the first cross-section measurement for the production of 2p2h states on argon. Using MicroBooNE data collected from the first three years of operation, we select events corresponding to a charged-current ν_μ interaction that left the argon nucleus in a 2p2h state. These interactions produce a topology with one muon and two protons in the final state (CC1μ2p0π). This analysis targets a single differential cross-section measurement for CC1μ2p0π event topologies in a variety of kinematic variables. Comparisons are made to a set of theoretical models that explore different cross-section modeling configurations.

*Email: MICROBOONE_INFO@fnal.gov

1 Introduction & Motivation

Since many current and next generation neutrino oscillation experiments will utilize dense nuclear targets, such as liquid argon (LAr), it is critical to characterize the impact of nuclear effects on neutrino cross-sections. One area of interest are neutrino events that eject 2 nucleons from the nucleus, leaving it with 2 holes: known as 2-particle 2-hole states (2p2h). The general picture is that the neutrino has a charged-current interaction with a neutron in the nucleus, producing a proton with significant momentum; this proton interacts with another proton, producing the 2p2h state. While the majority of 2p2h states are caused by Meson Exchange Currents (MEC) [1], some nuclear effects, such as Short-Range Nucleon-Nucleon correlations (SRC) [2], can also produce these states. In an accelerator-based liquid argon time projection chamber (LArTPC) experiment, such as MicroBooNE, a charged-current (CC) muon neutrino (ν_μ) interaction that results in a 2p2h state would have a final state topology of 1 muon, 2 protons, and no charged or neutral pions [3]. While there are existing measurements of CC1μ2p0π events on argon, the analyses were statistically limited and no cross-sections were extracted [4, 5]. This document presents the first single differential cross-section measurements of CC1μ2p0π topologies on argon, using data collected from the first 3 years of MicroBooNE operations.

2 The MicroBooNE Detector and Samples

MicroBooNE is a liquid argon time projection chamber (LArTPC) located at Fermi National Accelerator Laboratory. The detector sits on axis in the Booster Neutrino Beam (BNB) approximately 470 m from the neutrino production target. The detector consists of a cylindrical cryostat filled with 170 metric tons of liquid argon (active mass of 85 metric tons), 32 photomultiplier tubes (PMT), and a TPC that is 10.36 m long in the beam direction, 2.56 m wide in the drift direction, and 2.35 m tall [3].

Two data streams are recorded: on-beam (BNB) data that is collected in coincidence with a 1.6 μs BNB neutrino spill, and off-beam (EXT) data collected outside of the spill. The purpose of the EXT data is to characterize the cosmic ray background found in the detector.

To simulate neutrino events, MicroBooNE utilizes the GENIE neutrino event generator [6]. Using GENIE v3.0.6 G18_10a_02_11a [7] as the base modelset, parameters related to the shape and normalization of the CCQE and CC2p2h cross-sections were tuned to external data. The result of this tuning process is formally know as the MicroBooNE Tune [8]. Two samples of events are generated using the MicroBooNE Tune: (1) A sample in which the neutrino interaction occurs within the TPC, known as Overlay MC; (2) a sample in which the neutrino interaction occurs outside of the TPC, known as Dirt MC. The Overlay MC sample is used to develop reconstruction algorithms and event selections, while the Dirt MC sample is used to estimate backgrounds from neutrino interactions that occur outside of the TPC, but produce a signal within the detector. Simulated Overlay MC and Dirt MC events are overlaid on top of a subset of EXT data events to account for the cosmic ray background found in the BNB data.

In addition to the two samples mentioned above, another sample of overlay events is generated using the NuWro neutrino event generator [9]. For this sample, all the neutrino interactions occur within the TPC.

3 Event Selection

The goal of this analysis is to select events indicative of the production of a 2p2h state. We restrict ourselves to ν_μ CC interactions that produce exactly 1 muon and 2 protons in the final state. we utilize the Pandora framework to identify and reconstruct neutrino events [10]. A series of selection cuts are applied to the reconstructed objects to select CC1μ2p0π events.

First, the neutrino interaction vertex is required to be within a specified fiducial volume (FV), defined to be 10 cm from any TPC edge. We then require that the event contains exactly 3 objects identified as tracks and no objects identified as showers as determined by the Pandora reconstruction [11]. Additionally, the 3 tracks must each have a 3D distance between the reconstructed neutrino vertex and the reconstructed track start less than 4 cm to claim vertex attachment. We then make use of particle identification techniques described in Ref. [12] to identify the three tracks. Events are required to have a single identified muon and two identified protons.

The effectiveness of the event selection can be evaluated by considering the number of signal events selected from the Overlay MC sample. Using GENIE truth-level information, signal events are required to be ν_μ CC events that produce 1 muon with $0.1 \leq \mathrm{P}_\mu \leq 1.2\,\mathrm{GeV/c}$, 2 protons, both with $0.3 \leq \mathrm{P}_p \leq 1.0\,\mathrm{GeV/c}$, no charged pions with momentum above 65 MeV/c, no neutral pions of any momentum, and any number of neutrons. Adhering to this signal definition, the event selection described above achieves an efficiency of 13% and a purity 65.4%. Details of the event selection can be found in Ref. [13].

4 Theoretical Discussion

A study of simulated CC2p events generated from different model sets, each containing different Quasi-Elastic (QE) and Meson Exchange Curent (MEC) models, was conducted in order to determine variables with sensitivity to differences between the different models. We then extracted the single differential cross-sections from data as a function of these variables. The resulting cross-section from these simulated events are also compared with the data cross-sections.
In this analysis, we consider events generated from three combinations of models found within the GENIE neutrino event generator [6]. These model sets are listed below, along with the GENIE tune strings [7]. Note that each model set consists of a nuclear model, a QE model, an MEC model, and a final state interaction (FSI) model, where the specific combinations of nuclear, QE, and MEC models utilized are recommendations from the GENIE collaboration. It should be noted that all generated events were ν_μ charged-current (CC) interactions.

- G18_02a_00_000 : Relativistic Fermi Gas [14] + Lwellyn-Smith QE [15] + Empirical MEC [1] + hA2018 FSI [7, 16]
- G18_10a_02_11a: Local Fermi Gas [17] + Nieves/Valencia (QE + MEC) [18, 19] + hA2018 FSI [7, 16]
- G21_11b_00_000: Relativistic Mean Field Approximation [20, 21] + SuSAv2 (QE + MEC) [22, 23] + hN2018 FSI [7, 24]

These particular model sets were chosen to understand the effect of different model sets on the shape of 2p2h cross-sections. While MECs are the main contributors to 2p2h states, QE can also lead to 2p2h states with the inclusion of FSI effects. Each model set contains the most utilized QE and MEC models found withint GENIE.
Four cuts are applied at the truth level to select events from each sample that were consistent with the signal definition provided in Section 3. Selected events contained 1 muon with momentum between 0.1 and 1.2 GeV/c, 2 protons with momenta between 0.3 and 1.0 GeV/c, 0 charged pions with momenta above 65 MeV/c, and 0 neutral pions of any momentum. Note that the proton with the most momentum is labeled as the leading proton and the secondary proton is labeled as the recoil proton. Selected events from each model set were plotted as a function of a variety of physics variables. For the purpose of identifying variables that are most sensitive to the differences between models, distributions from each model set were area normalized to allow for direct comparisons. This allowed for differences in predictions from each model set to be easily identified.
Two variables identified as being sensitive to differences between the model sets are the opening angle between the protons in the lab frame (denoted γ_{Lab}), and the opening angle between the muon and total proton momentum vector (denoted $\gamma_{\mu,\mathrm{p_L}+\mathrm{p_R}}$). Schematic diagrams of these angles can be found in Figure 1.

5 Cross-Section Unfolding

The single differential cross-sections are extracted using D'Agostini iterative Bayesian unfolding [25, 26] in order to report cross-sections as a function of truth-level values. The extracted data cross section in a true bin T (Data $_{\mathrm{T}}$) can be calculated using the following formula:

$$\text{Data}_{\mathrm{T}} = \sum_{\mathrm{R}} \mathrm{U}_{\mathrm{T,R}} \times (\text{Data}_{\mathrm{R}} - \text{Backgrounds}_{\mathrm{R}}) \tag{1}$$

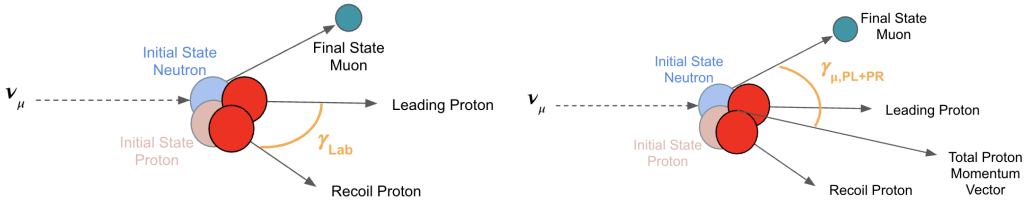

Figure 1: Diagrams of γ_{Lab} (left) and $\gamma_{\mu,\text{p}_\text{L}+\text{p}_\text{R}}$ (right).

where Data $_\text{T}$ is the data cross-section in a true bin T (also known as the posterior), $\text{U}_{\text{T,R}}$ is an unfolding matrix, and Data $_\text{R}$ and Backgrounds $_\text{R}$ are the measured data and background events in reconstructed bin R, respectively. The unfolding matrix is then constructed as such:

$$\text{U}_{\text{T,R}} = \frac{\text{S}_{\text{T,R}} \times \text{P}_\text{T}}{\sum_\text{R} \text{S}_{\text{T,R}} \times \text{P}_\text{T}} \tag{2}$$

where $\text{S}_{\text{T,R}}$ is the smearing matrix and P_T is known as the prior: both of which will be discussed below. The smearing matrix is a 2D histogram that describes how the reconstruction smears truth level quantities into reconstructed quantities. The smearing matrix is created from a more rudimentary object known as the migration matrix M: a 2D histogram that describes the migration of truth level values into reconstructed values. The migration is filled with the reconstructed and truth level values of a specific variable for true CC1μ2p0π events that were reconstructed in the Overlay MC. The smearing matrix is then calculated from the migration matrix by normalizing the reconstruction rows:

$$\text{S}_{\text{T,R}} = \frac{\text{M}_{\text{T,R}}}{\sum_\text{t} \text{M}_{\text{t,R}}} \tag{3}$$

where $\text{S}_{\text{T,R}}$ is the smearing matrix value in true bin T and reconstructed bin R, $\text{M}_{\text{T,R}}$ is the migration matrix value in true bin T and reconstructed bin R, and $\text{M}_{\text{t,R}}$ is the value of the migration matrix in true bin t and reconstructed bin R. The interpretation is that $S_{\text{T,R}}$ is the probability for a reconstructed event in bin R to have come from true bin T.

The prior is the first estimate for the true distribution. RooUnfold [27], the software utilized by this analysis to employ the D'Agostini method, assumes that the initial prior is a 1D projection of the smearing matrix onto the true axis. Since this initial prior is not always an accurate representation of the truth distribution, we iterate over Equation 2 by using the posterior as the new prior in the next calculation. The iterative method typically only takes 3-4 iterations before convergence is achieved. We determine the optimal number of iterations using techniques described in Ref. [28]. We utilize two iterations to unfold the distribution for $\cos(\gamma_{\text{Lab}})$ and four iterations to unfold the distribution for $\cos(\gamma_{\mu,\text{p}_\text{L}+\text{p}_\text{R}}$).

6 Results and Conclusions

Distributions of selected events as a function of the cosine of γ_{Lab} (top) and $\gamma_{\mu,\text{p}_\text{L}+\text{p}_\text{R}}$ (bottom) can be found in Figure 2. The black points represent events selected from BNB data, the purple hashed histogram represents events selected from EXT data, the brown represents events selected from Dirt MC, and the other colors represents events selected from Overlay MC. The error bars on the data points are purely statistical while the hashed lines represent the $\pm 1\sigma$ on the combination of the Overlay MC, Dirt MC, and EXT data (also known as the prediction). Events selected from the Overlay MC sample are subdivided into different final state topologies (plots on the left) or different interaction modes (right) based on truth information. We find that our CC1μ2p0π signal (represented by the pink band in the plots on the left) represents the majority of events selected from the Overlay-MC sample. We also find that the CCMEC (represented by the magenta band in the plots on the right) has a somewhat different shape compared to our signal. This is expected as MEC is not the only contributor to CC1μ2p0π topologies.

Contributions from flux modeling and POT counting [29], re-interaction modeling [30], cross-section modeling [8], detector modeling [31], and dirt modeling are considered in the calculation of the systematic uncertainties. Of these six sources of systematic uncertainties, cross-section modeling and detector modeling provide the largest sources of systematic error.

When comparing the BNB data with events selected from a combination of EXT data, Overlay MC, and Dirt MC, we generally find good shape agreement as well as normalization agreement at the 1σ level. However, we find an overall shape disagreement between the BNB data and the backgrounds for both variables. In $\cos(\gamma_{\mathrm{Lab}})$, we find the shape disagreement in the region -1 $\leq \cos(\gamma_{\mathrm{Lab}}) \leq$ -0.25. In $\cos(\gamma_{\mu,\mathrm{p_L+p_R}})$, we find that the data clearly peaks in the region $0 \leq \cos(\gamma_{\mu,\mathrm{p_L+p_R}}) \leq 0.25$, while the background peaks in the region $0 \leq \cos(\gamma_{\mu,\mathrm{p_L+p_R}}) \leq 0.5$.

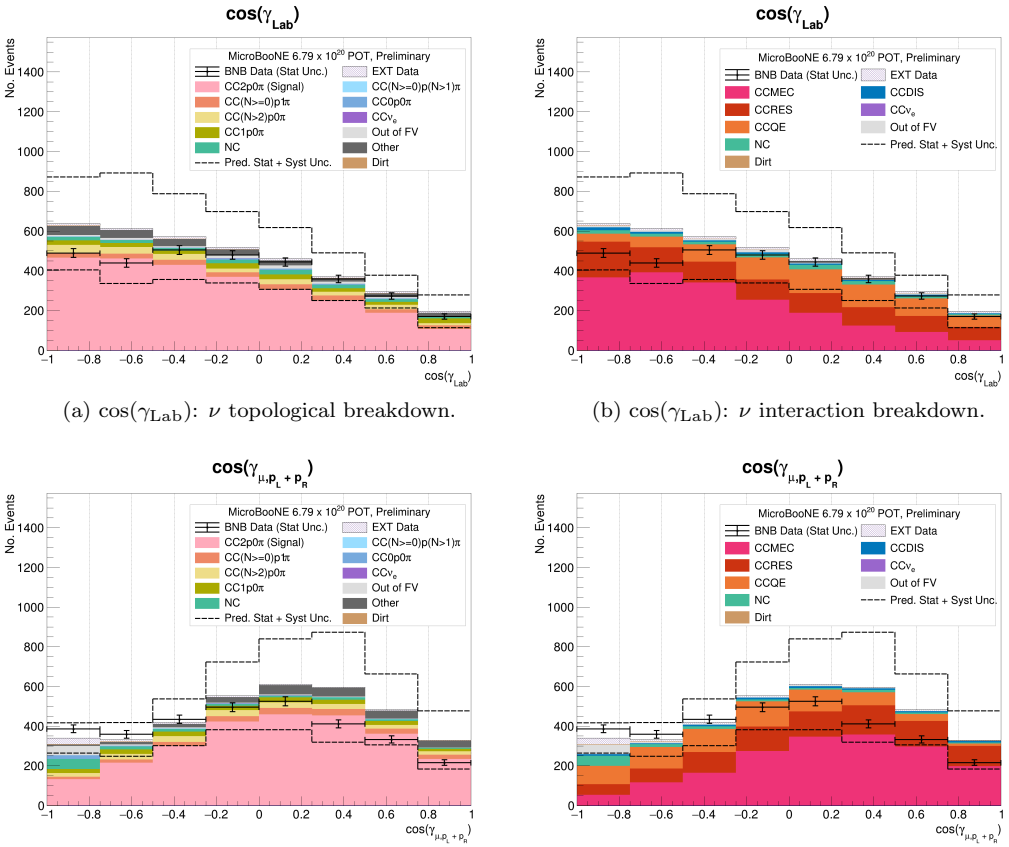

(a) $\cos(\gamma_{\mathrm{Lab}})$: ν topological breakdown.

(b) $\cos(\gamma_{\mathrm{Lab}})$: ν interaction breakdown.

(c) $\cos(\gamma_{\mu,\mathrm{p_L+p_R}})$: ν topological breakdown.

(d) $\cos(\gamma_{\mu,\mathrm{p_L+p_R}})$: ν interaction breakdown.

Figure 2: $\cos(\gamma_{\mathrm{Lab}})$ and $\cos(\gamma_{\mu,\mathrm{p_L+p_R}})$. Plots on the left show MC broken down into ν topological breakdown. Plots on the right show MC broken down into ν channels. The error bars on the data points are purely statistical while the hashed lines represent the $\pm 1\sigma$ on the combination of the Overlay MC, Dirt MC, and EXT data (also known as the prediction).

In addition to the event distributions, we also display the single differential cross-sections as a function of the cosine of γ_{Lab} (left) and $\gamma_{\mu,\mathrm{p_L+p_R}}$ (right) in Figure 3. The black points represent the extracted cross-section from BNB data where the inner error bands represent the statistical uncertainty and the outer error bands represent the systematic uncertainty. Each colored curve represents the extracted cross-section from a particular model set. The cross-sections for the Empirical, Nieves, and SuSAv2 model sets were derived using the method described in [32]. The MicroBooNE Tune and NuWro cross-section curves were created by selecting generated CC1μ2p0π signal events from the Overlay MC and NuWro samples, respectively. Each distribution was then normalized by the number of target nucleons and the total integrated flux to produce a cross-section curve. The χ^2/DoF between a particular model curve and the data, with consideration for

systematic and statistical uncertainty, is shown in the parentheses in the plot legends.

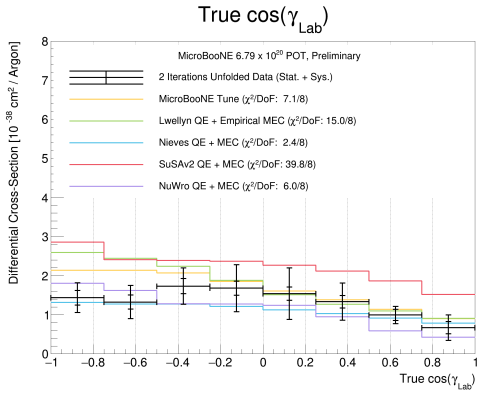

(a) $\cos(\gamma_{\mathrm{Lab}})$. The inner error bands represent the statistical uncertainty and the outer error bands represent the systematic uncertainty. The χ^2/DoF is calculated for each model set and shown in the parentheses in the legend.

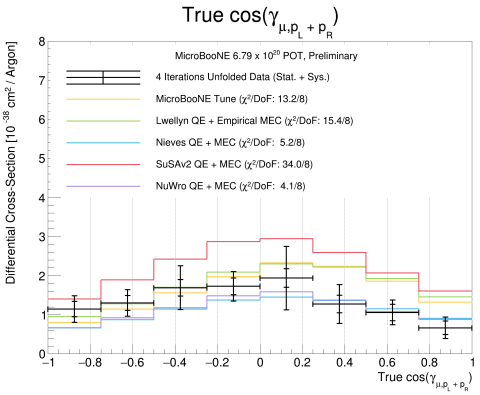

(b) $\cos(\gamma_{\mu,\mathrm{p_L}+\mathrm{p_R}})$ The inner error bands represent the statistical uncertainty and the outer error bands represent the systematic uncertainty. The χ^2/DoF is calculated for each model set and shown in the parentheses in the legend.

Figure 3: Resulting differential cross section for $\cos(\gamma_{\mathrm{Lab}})$ and $\cos(\gamma_{\mu,\mathrm{p_L}+\mathrm{p_R}})$. Statistical and systematic errors are included.

We find that the SuSAv2 cross-section prediction is higher than other models, and often does not agree with data at the 1σ level. This is unsurprising since the the superscaling approach (where super scaling functions derived from relativistic assumptions are used to scale the cross-section at high momentum transfers) begins to break down for smaller neutrino energies, as discussed in [23, 22].

We find that the Nieves model and the NuWro model have the best χ^2/DoF for $\cos(\gamma_{\mathrm{Lab}})$. However, if we consider the region of $-1.0 \leq \cos(\gamma_{\mathrm{Lab}}) \leq -0.5$, we find that the Nieves model and NuWro are within 1σ of the data while the MicroBooNE tune, the Nieves model, and NuWro are barely within 1σ for the region of $-0.5 \leq \cos(\gamma_{\mathrm{Lab}}) \leq -0.25$.

For the results plotted vs. $\cos(\gamma_{\mu,\mathrm{p_L}+\mathrm{p_R}})$, we again find thta NuWro and Nieves produce the best χ^2/DoF. In the region of $0.25 \leq \cos(\gamma_{\mu,\mathrm{p_L}+\mathrm{p_R}}) \leq 1.0$, we find that the Nieves model and NuWro model are once again within 1σ of the data.

The MicroBooNE Tune uses all the same model elements as the Nieves sample, but contains 4 tuned parameters, including the CC2p2h cross-section normalization. The overall normalization difference between the MicroBooNE tune and the Nieves model for both variables is most likely caused by the tuning of this variable. Further, the slight differences between the shape of these distributions could come about from any of the tuned parameters.

The NuWro prediction uses the same nuclear and MEC model as the Nieves sample, but uses the Llewellyn-Smith QE model, which does not include Coulombic effects [33] or Long-Range Nucleon-Nucleon correlations (LRC) [34]. The exclusion of both these effects is likely what leads to the differences we observe between these two curves.

In conclusion, we presented the first measurement of single differential cross-sections as a function of $\cos(\gamma_{\mathrm{Lab}})$ and $\cos(\gamma_{\mu,\mathrm{p_L}+\mathrm{p_R}})$. The cross-sections are extracted from data using the D'Agostini Bayesian unfolding method as implemented in the RooUnfold framework. We find a varied amount of shape and normalization agreement between the data and predictions from several different model sets. None of the models reproduce the exact shape of the data which may come about from the absence in modeling of contributions from SRCs.

References

[1] Teppei Katori. Meson Exchange Current (MEC) Models in Neutrino Interaction Generators. *AIP Conf. Proc.*, 1663(1):030001, 2015.

[2] Lonardoni D. Weiss R. et al. Cruz-Torres, R. Many-body factorization and position–momentum equivalence of nuclear short-range correlations. *Nat. Phys.*, 17:306–310, September 2020.

[3] R. Acciarri et al. Design and Construction of the MicroBooNE Detector. *JINST*, 12(02):P02017, 2017.

[4] R. Acciarri et al. Detection of back-to-back proton pairs in charged-current neutrino interactions with the argoneut detector in the numi low energy beam line. *Phys. Rev. D*, 90:012008, Jul 2014.

[5] Selection of ν_μ charged–current induced interactions with n$\geq$0 protons and performance of events with n=2 protons in the final state in the microboone detector from the bnb. https://microboone.fnal.gov/wp-content/uploads/MICROBOONE-NOTE-1056-PUB.pdf.

[6] C. Andreopoulos et al. The GENIE Neutrino Monte Carlo Generator. *Nucl. Instrum. Meth. A*, 614:87–104, 2010.

[7] Luis Alvarez-Ruso et al. Recent highlights from GENIE v3. *Eur. Phys. J. ST*, 230(24):4449–4467, 2021.

[8] P. Abratenko et al. New $CC0\pi$ GENIE model tune for MicroBooNE. *Phys. Rev. D*, 105(7):072001, 2022.

[9] T. Golan, J. T. Sobczyk, and J. Zmuda. NuWro: the Wroclaw Monte Carlo Generator of Neutrino Interactions. *Nucl. Phys. B Proc. Suppl.*, 229-232:499–499, 2012.

[10] R. Acciarri et al. The Pandora multi-algorithm approach to automated pattern recognition of cosmic-ray muon and neutrino events in the MicroBooNE detector. *Eur. Phys. J. C*, 78(1):82, 2018.

[11] Wouter Van De Pontseele. *Search for Electron Neutrino Anomalies with the MicroBooNE Detector*. PhD thesis, Oxford U., 2020.

[12] P. Abratenko et al. Calorimetric classification of track-like signatures in liquid argon TPCs using MicroBooNE data. *JHEP*, 12:153, 2021.

[13] MicroBooNE Collaboration. Study of CC2p0π Event Topologies in the Microboone Detector. https://microboone.fnal.gov/wp-content/uploads/MICROBOONE-NOTE-1096-PUB.pdf, 2021.

[14] R. A. Smith and E. J. Moniz. NEUTRINO REACTIONS ON NUCLEAR TARGETS. *Nucl. Phys. B*, 43:605, 1972. [Erratum: Nucl.Phys.B 101, 547 (1975)].

[15] C. H. Llewellyn Smith. Neutrino Reactions at Accelerator Energies. *Phys. Rept.*, 3:261–379, 1972.

[16] D. Ashery, I. Navon, G. Azuelos, H. K. Walter, H. J. Pfeiffer, and F. W. Schlepütz. True absorption and scattering of pions on nuclei. *Phys. Rev. C*, 23:2173–2185, May 1981.

[17] J. Nieves, J. E. Amaro, and M. Valverde. Inclusive quasielastic charged-current neutrino-nucleus reactions. *Phys. Rev. C*, 70:055503, Nov 2004.

[18] J. Nieves, F. Sanchez, I. Ruiz Simo, and M. J. Vicente Vacas. Neutrino Energy Reconstruction and the Shape of the CCQE-like Total Cross Section. *Phys. Rev. D*, 85:113008, 2012.

[19] Jackie Schwehr, Dan Cherdack, and Rik Gran. GENIE implementation of IFIC Valencia model for QE-like 2p2h neutrino-nucleus cross section https://arxiv.org/pdf/1601.02038.pdf. 2016.

[20] Brian D. Serot and John Dirk Walecka. *Relativistic Nuclear Many-Body Theory*, pages 49–92. Springer US, Boston, MA, 1992.

[21] J. A. Caballero, J. E. Amaro, M. B. Barbaro, T. W. Donnelly, C. Maieron, and J. M. Udias. Superscaling in charged current neutrino quasielastic scattering in the relativistic impulse approximation. *Phys. Rev. Lett.*, 95:252502, Dec 2005.

[22] S. Dolan, G. D. Megias, and S. Bolognesi. Implementation of the susav2-meson exchange current 1p1h and 2p2h models in genie and analysis of nuclear effects in t2k measurements. *Phys. Rev. D*, 101:033003, Feb 2020.

[23] T. W. Donnelly and Ingo Sick. Superscaling in inclusive electron - nucleus scattering. *Phys. Rev. Lett.*, 82:3212–3215, 1999.

[24] L. A. Harewood and R. Gran. Elastic hadron-nucleus scattering in neutrino-nucleus reactions and transverse kinematics measurements https://arxiv.org/pdf/1906.10576.pdf. 6 2019.

[25] G. D'Agostini. Improved iterative bayesian unfolding, 2010.

[26] G. D'Agostini. A multidimensional unfolding method based on bayes' theorem. *Nuclear Instruments and Methods in Physics Research Section A: Accelerators, Spectrometers, Detectors and Associated Equipment*, 362(2):487–498, 1995.

[27] Tim Adye. Unfolding algorithms and tests using RooUnfold. In *PHYSTAT 2011*, pages 313–318, Geneva, 2011. CERN.

[28] S. Dolan. What we measure when we measure σ. https://indico.cern.ch/event/703880/contributions/3157171/attachments/1733799/2803379/dolan_funfolding.pdf, 2018.

[29] A. A. Aguilar-Arevalo et al. First measurement of the muon antineutrino double-differential charged-current quasielastic cross section. *Phys. Rev. D*, 88:032001, Aug 2013.

[30] J. Calcutt, C. Thorpe, K. Mahn, and Laura Fields. Geant4Reweight: a framework for evaluating and propagating hadronic interaction uncertainties in Geant4. *JINST*, 16(08):P08042, 2021.

[31] P. Abratenko et al. Novel approach for evaluating detector-related uncertainties in a LArTPC using MicroBooNE data. *Eur. Phys. J. C*, 82(5):454, 2022.

[32] Steven Gardiner. Simulating low-energy neutrino interactions with MARLEY. *Comput. Phys. Commun.*, 269:108123, 2021.

[33] Jonathan Engel. Approximate treatment of lepton distortion in charged-current neutrino scattering from nuclei. *Phys. Rev. C*, 57:2004–2009, Apr 1998.

[34] K. Amir-Azimi-Nili, H. Muther, L. D. Skouras, and A. Polls. Long range correlations and the momentum distribution in nuclei. *Nucl. Phys. A*, 604:245–262, 1996.